

Differential Kronecker Product Beamforming

Israel Cohen , *Fellow, IEEE*, Jacob Benesty , and Jingdong Chen , *Senior Member, IEEE*

Abstract—Differential beamformers have attracted much interest over the past few decades. In this paper, we introduce differential Kronecker product beamformers that exploit the structure of the steering vector to perform beamforming differently from the well-known and studied conventional approach. We consider a class of microphone arrays that enable to decompose the steering vector as a Kronecker product of two steering vectors of smaller virtual arrays. In the proposed approach, instead of directly designing the differential beamformer, we break it down following the decomposition of the steering vector, and show how to derive differential beamformers using the Kronecker product formulation. As demonstrated, the Kronecker product decomposition facilitates further flexibility in the design of differential beamformers and in the tradeoff control between the directivity factor and the white noise gain.

Index Terms—Differential beamforming, Kronecker product, microphone array, superdirective beamforming, beampattern, white noise gain, directivity factor, front-to-back ratio.

I. INTRODUCTION

KRONECKER product decompositions have been recently investigated in the context of acoustic imaging [1], [2], linear system identification [3], [4], and beamforming [5], [6]. Ribeiro and Nascimento [1] considered the problem of acoustic imaging using planar microphone arrays. They introduced the Kronecker array transform, which enables the acceleration of acoustic imaging techniques, essentially by reorganizing the matrix-vector multiplication structure for a special case of separable arrays. They showed that for planar arrays with a rectangular grid of microphones, the Kronecker array transform enables to reconstruct acoustic images more accurately and with higher resolutions than standard methods. This transform, which was originally designed for acoustic camera applications, was later generalized for compressive beamforming by Nascimento *et al.* [2].

Recently, Paleologu *et al.* [4] addressed the problem of linear system identification by using approximate Kronecker product

Manuscript received September 8, 2018; revised December 25, 2018; accepted January 20, 2019. Date of publication January 24, 2019; date of current version March 28, 2019. This work was supported in part by the Israel Science Foundation under Grant 576/16 and in part by the ISF-NSFC joint research program under Grants 2514/17 and 61761146001. The associate editor coordinating the review of this manuscript and approving it for publication was Dr. Richard Christian Hendriks. (*Corresponding author: Israel Cohen.*)

I. Cohen is with the Andrew and Erna Viterby Faculty of Electrical Engineering, Technion—Israel Institute of Technology, Haifa 3200003, Israel (e-mail: icohen@ee.technion.ac.il).

J. Benesty is with the INRS-EMT, University of Quebec, Montreal, QC H5A 1K6, Canada (e-mail: benesty@emt.inrs.ca).

J. Chen is with the Northwestern Polytechnical University, Xi'an 710072, China (e-mail: jingdongchen@ieec.org).

Digital Object Identifier 10.1109/TASLP.2019.2895241

(KP) decompositions of the impulse response. They proposed to estimate optimal KP decompositions of the impulse response based on an iterative Wiener filter, which compared to the conventional Wiener filter, is computationally more efficient and yields better performances using less amount of data to estimate the statistics. They showed that finding an optimal KP decomposition of the impulse response is generally useful for real-world acoustic echo cancellation applications.

Differential beamformers [7]–[9] are a particular important class of fixed beamformers, which yield the highest gains in diffuse noise. Differential microphone arrays are generally small in size, and their beampatterns are almost frequency invariant, which is critical when we deal with broadband signals such as speech. Consequently, optimal designs of differential beamformers have attracted much interest over the past few decades.

In this paper, we introduce differential KP beamformers that take advantage of the steering vector structure to perform beamforming differently from the well-known and studied conventional approach. The conventional way of doing beamforming is by applying in the frequency domain a complex-valued linear filter, \mathbf{h} , of length M to the observation signal vector, where M is the number of microphones in the array. With the conventional beamforming approach, M coefficients of \mathbf{h} need to be estimated for each frequency bin. We consider a particular class of microphone arrays that enable to decompose the steering vector as a Kronecker product of two steering vectors of smaller virtual arrays [1], [5], [10]. That is, arrays of $M = M_1 M_2$ microphones that can be configured from replications of one virtual array (containing M_1 microphones) to the microphone positions of the other virtual array (containing M_2 microphones). In this case, the steering vector (of length M) can be decomposed as

$$\mathbf{d} = \mathbf{d}_1 \otimes \mathbf{d}_2, \quad (1)$$

where \otimes is the Kronecker product, \mathbf{d}_1 is the steering vector (of length M_1) corresponding to a virtual array of M_1 microphones, and \mathbf{d}_2 is the steering vector (of length M_2) corresponding to another virtual array of M_2 microphones. Note that (1) is satisfied whenever the physical array can be obtained from replications of one virtual array to the microphone positions of the other virtual array (see e.g., Fig. 1).

In the proposed approach, instead of directly designing the filter \mathbf{h} of length M , we break it down following the decomposition of the global steering vector as

$$\mathbf{h} = \mathbf{h}_1 \otimes \mathbf{h}_2, \quad (2)$$

where \mathbf{h}_1 and \mathbf{h}_2 are two complex-valued linear filters of lengths M_1 and M_2 , respectively. With this method, we need to

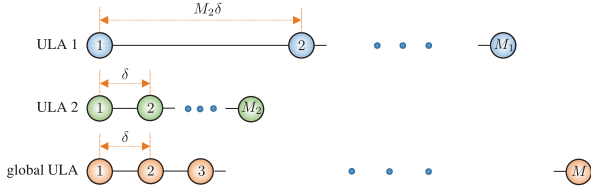


Fig. 1. Illustration of ULA 1 with M_1 microphones and an interelement spacing equal to $M_2\delta$, ULA 2 with M_2 microphones and an interelement spacing equal to δ , and global ULA with $M = M_1M_2$ microphones and an interelement spacing equal to δ .

estimate $M_1 + M_2$ coefficients [M_1 for \mathbf{h}_1 and M_2 for \mathbf{h}_2] instead of $M = M_1M_2$ for the conventional technique. This generally implies smaller matrices to invert (increasing robustness) [8], [11].

There are many ways to optimize the coefficients of \mathbf{h}_1 and \mathbf{h}_2 depending on what we want and the application at hand. We introduce differential KP beamformers, and show how to derive such beamformers, as well as new approaches through the designs of \mathbf{h}_1 and \mathbf{h}_2 . We show that using the KP decomposition, the global beampattern can be expressed as the product of the beampatterns of the two virtual arrays. Also, the white noise gain of the global array can be expressed as the product of the white noise gains of the two virtual arrays, while the directivity factor and the front-to-back ratio of the global array cannot be factorized. We demonstrate designs of very flexible differential KP beamformers by exploiting these interesting properties.

The rest of the paper is organized as follows. In Section II, we introduce the KP decomposition of a physical array into two virtual arrays and present the signal model. In Section III, we formulate the problem of KP beamforming. In Section IV, we define some important performance measures by using KP filters. Then, in Section V, we show how to derive differential beamformers using the KP formulation.

II. SIGNAL MODEL

We consider two different virtual uniform linear arrays (ULAs) on the same line denoted 1 and 2. ULA 1 has M_1 microphones and an interelement spacing equal to $M_2\delta$, where δ is some unit spacing, and ULA 2 has M_2 microphones and an interelement spacing equal to δ (see Fig. 1). Assume that a desired source signal (plane wave), in the farfield, propagates from the azimuth angle, θ , in an anechoic acoustic environment at the speed of sound, i.e., $c = 340$ m/s, and impinges on the above described virtual arrays. In this scenario, the corresponding steering vectors (of lengths M_1 and M_2 , respectively) are [12]

$$\mathbf{d}_{1,\theta}(\omega) = [1 \ e^{-jM_2\varpi \cos \theta} \ \dots \ e^{-j(M_1-1)M_2\varpi \cos \theta}]^T, \quad (3)$$

$$\mathbf{d}_{2,\theta}(\omega) = [1 \ e^{-j\varpi \cos \theta} \ \dots \ e^{-j(M_2-1)\varpi \cos \theta}]^T, \quad (4)$$

where the superscript T is the transpose operator, j is the imaginary unit,

$$\varpi = \frac{\omega\delta}{c}, \quad (5)$$

$\omega = 2\pi f$ is the angular frequency, and $f > 0$ is the temporal frequency. In this study, we are interested in the physical linear array whose associated steering vector is of the form:

$$\mathbf{d}_\theta(\omega) = \mathbf{d}_{1,\theta}(\omega) \otimes \mathbf{d}_{2,\theta}(\omega). \quad (6)$$

The corresponding physical ULA consists of $M = M_1M_2$ microphones with an interelement spacing equal to δ . We will refer to this array as the global or whole ULA. We consider doing beamforming with small values of δ [7], [8], [13], where the main lobe is at the angle $\theta = 0$ (endfire direction) and the desired signal propagates from the same angle. Beamforming under these conditions has the potential to lead to large array gains. Our objective is to study differential beamforming with the proposed ULAs.

Since the source propagates from the angle $\theta = 0$, the observation signal vector of length M_1M_2 can be expressed in the frequency domain as [11], [14]

$$\begin{aligned} \mathbf{y}(\omega) &= [Y_1(\omega) \ Y_2(\omega) \ \dots \ Y_M(\omega)]^T \\ &= \mathbf{x}(\omega) + \mathbf{v}(\omega) \\ &= \mathbf{d}_0(\omega) X(\omega) + \mathbf{v}(\omega), \end{aligned} \quad (7)$$

where $Y_m(\omega)$ is the m th microphone signal, $\mathbf{x}(\omega) = \mathbf{d}_0(\omega) X(\omega)$, $X(\omega)$ is the zero-mean desired source signal, $\mathbf{d}_0(\omega) = \mathbf{d}_{1,0}(\omega) \otimes \mathbf{d}_{2,0}(\omega)$ is the steering vector at $\theta = 0$ (direction of the desired source), $\mathbf{v}(\omega)$ is the zero-mean additive noise signal vector defined similarly to $\mathbf{y}(\omega)$, and $X(\omega)$ and $\mathbf{v}(\omega)$ are uncorrelated. In the rest, in order to simplify the notation, we drop the dependence on the angular frequency, ω . So, for example, (7) is written as $\mathbf{y} = \mathbf{d}_0 X + \mathbf{v}$. We deduce that the covariance matrix of \mathbf{y} is

$$\begin{aligned} \Phi_{\mathbf{y}} &= E(\mathbf{y}\mathbf{y}^H) \\ &= \Phi_{\mathbf{x}} + \Phi_{\mathbf{v}}, \end{aligned} \quad (8)$$

where $E(\cdot)$ denotes mathematical expectation, the superscript H is the conjugate-transpose operator,

$$\begin{aligned} \Phi_{\mathbf{x}} &= \phi_X \mathbf{d}_0 \mathbf{d}_0^H \\ &= \phi_X (\mathbf{d}_{1,0} \otimes \mathbf{d}_{2,0}) (\mathbf{d}_{1,0} \otimes \mathbf{d}_{2,0})^H \\ &= \phi_X (\mathbf{d}_{1,0} \mathbf{d}_{1,0}^H) \otimes (\mathbf{d}_{2,0} \mathbf{d}_{2,0}^H) \end{aligned} \quad (9)$$

is the covariance matrix of \mathbf{x} , with $\phi_X = E(|X|^2)$ being the variance of X , and $\Phi_{\mathbf{v}} = E(\mathbf{v}\mathbf{v}^H)$ is the covariance matrix of \mathbf{v} . Assuming that the first microphone is the reference, we can express (8) as

$$\Phi_{\mathbf{y}} = \phi_X \mathbf{d}_0 \mathbf{d}_0^H + \phi_{V_1} \Gamma_{\mathbf{v}}, \quad (10)$$

where $\phi_{V_1} = E(|V_1|^2)$ is the variance of the noise at the reference microphone and $\Gamma_{\mathbf{v}} = \Phi_{\mathbf{v}}/\phi_{V_1}$ is the pseudo-coherence matrix of the noise. In the case of the spherically isotropic (diffuse) noise field, which will often be assumed here, (10) becomes

$$\Phi_{\mathbf{y}} = \phi_X \mathbf{d}_0 \mathbf{d}_0^H + \phi \Gamma, \quad (11)$$

where ϕ is the variance of the diffuse noise and

$$\Gamma = \frac{1}{2} \int_0^\pi \mathbf{d}_\theta \mathbf{d}_\theta^H \sin \theta d\theta. \quad (12)$$

It can be verified that the elements of the $M \times M$ matrix $\Gamma(\omega)$ are

$$\begin{aligned} [\Gamma(\omega)]_{mn} &= \frac{\sin[(m-n)\varpi]}{(m-n)\varpi} \\ &= \text{sinc}[(m-n)\varpi], \end{aligned} \quad (13)$$

with $[\Gamma(\omega)]_{mm} = 1$, $m = 1, 2, \dots, M$.

One of our main objectives in this study is to take advantage of the global ULA steering vector structure in the particular case of $M = M_1 M_2$ to perform beamforming differently from the well-known and studied conventional approach. It will be demonstrated that the new technique is very flexible.

III. KRONECKER PRODUCT BEAMFORMING

The conventional way of doing beamforming is by applying a complex-valued linear filter, \mathbf{h} , of length M to the observation signal vector, \mathbf{y} . This processing is [11]

$$Z = \mathbf{h}^H \mathbf{y}, \quad (14)$$

where Z is the estimate of the desired signal, X . In order to fully exploit the structure of the global steering vector, let us consider the complex-valued filters having the form:

$$\mathbf{h} = \mathbf{h}_1 \otimes \mathbf{h}_2, \quad (15)$$

where \mathbf{h}_1 and \mathbf{h}_2 are two complex-valued linear filters of lengths M_1 and M_2 , respectively. In other words, the global beamformer, \mathbf{h} , follows the decomposition of the global steering vector, \mathbf{d}_θ . In the proposed approach, beamforming is performed by applying \mathbf{h} [as defined in (15)] to \mathbf{y} [from (7)]. We get

$$\begin{aligned} Z &= \mathbf{h}^H \mathbf{y} \\ &= \mathbf{h}^H \mathbf{d}_0 X + \mathbf{h}^H \mathbf{v} \\ &= X_{\text{fd}} + V_{\text{rn}}, \end{aligned} \quad (16)$$

where Z is the estimate of the desired signal, X ,

$$\begin{aligned} X_{\text{fd}} &= (\mathbf{h}_1 \otimes \mathbf{h}_2)^H (\mathbf{d}_{1,0} \otimes \mathbf{d}_{2,0}) X \\ &= (\mathbf{h}_1^H \mathbf{d}_{1,0}) (\mathbf{h}_2^H \mathbf{d}_{2,0}) X \end{aligned} \quad (17)$$

is the filtered desired signal, and

$$V_{\text{rn}} = (\mathbf{h}_1 \otimes \mathbf{h}_2)^H \mathbf{v} \quad (18)$$

is the residual noise. We deduce that the variance of Z is

$$\begin{aligned} \phi_Z &= \phi_X |\mathbf{h}_1^H \mathbf{d}_{1,0}|^2 |\mathbf{h}_2^H \mathbf{d}_{2,0}|^2 \\ &\quad + \phi_{V_1} (\mathbf{h}_1 \otimes \mathbf{h}_2)^H \Gamma_{\mathbf{v}} (\mathbf{h}_1 \otimes \mathbf{h}_2). \end{aligned} \quad (19)$$

We see that with this method, we only need to estimate $M_1 + M_2$ coefficients (M_1 for \mathbf{h}_1 and M_2 for \mathbf{h}_2) instead of $M_1 M_2$ for the conventional technique. This generally implies smaller matrices to invert (increasing robustness) [8], [11]. Notice that this way of doing beamforming may not be completely new.

A similar approach was proposed in [5], but in the context of multiple-input and multiple-output (MIMO) radar applications.

In our context, the distortionless constraint in the direction of the desired source, i.e., $\theta = 0$, is often required, i.e.,

$$\mathbf{h}^H \mathbf{d}_0 = (\mathbf{h}_1^H \mathbf{d}_{1,0}) (\mathbf{h}_2^H \mathbf{d}_{2,0}) = 1. \quad (20)$$

Therefore, we may choose $\mathbf{h}_1^H \mathbf{d}_{1,0} = \mathbf{h}_2^H \mathbf{d}_{2,0} = 1$, so that (20) is satisfied. [In some applications, it may be useful to design \mathbf{h}_1 and \mathbf{h}_2 such that $\mathbf{h}_1^H \mathbf{d}_{1,0}$ varies as a function of frequency, while (20) is still satisfied, but we do not consider this here.]

IV. PERFORMANCE MEASURES

In this section, we define some important performance measures by using KP filters.

The first useful measure discussed in this section is the beam-pattern or directivity pattern, which describes the sensitivity of the beamformer to a plane wave (source signal) impinging on the global ULA from the direction θ . Mathematically, it is defined as

$$\begin{aligned} \mathcal{B}_\theta(\mathbf{h}) &= \mathbf{d}_\theta^H \mathbf{h} \\ &= (\mathbf{d}_{1,\theta}^H \mathbf{h}_1) (\mathbf{d}_{2,\theta}^H \mathbf{h}_2) \\ &= \mathcal{B}_{1,\theta}(\mathbf{h}_1) \times \mathcal{B}_{2,\theta}(\mathbf{h}_2), \end{aligned} \quad (21)$$

where

$$\begin{aligned} \mathcal{B}_{i,\theta}(\mathbf{h}_i) &= \mathbf{d}_{i,\theta}^H \mathbf{h}_i \\ &= \sum_{m=1}^{M_i} H_{i,m} e^{j(m-1)\varpi_i \cos \theta} \end{aligned} \quad (22)$$

for $i = 1, 2$ are the beampatterns of the virtual ULAs, with $\varpi_1 = M_2 \varpi$, $\varpi_2 = \varpi$, and $H_{i,m}$, $m = 1, 2, \dots, M_i$ being the coefficients of \mathbf{h}_i . Let $\mathcal{Z}_i = e^{j\varpi_i \cos \theta}$ for $i = 1, 2$, we can express the global beampattern as a polynomial in two variables, which is the product of two polynomials (of degrees $M_1 - 1$ and $M_2 - 1$) in one variable each, i.e.,

$$\begin{aligned} \mathcal{B}(\mathcal{Z}_1, \mathcal{Z}_2) &= \mathcal{B}_1(\mathcal{Z}_1) \times \mathcal{B}_2(\mathcal{Z}_2) \\ &= \left(\sum_{m_1=1}^{M_1} H_{1,m_1} \mathcal{Z}_1^{m_1-1} \right) \left(\sum_{m_2=1}^{M_2} H_{2,m_2} \mathcal{Z}_2^{m_2-1} \right). \end{aligned} \quad (23)$$

From this perspective, we can see that this beampattern has at most $M_1 + M_2 - 2$ distinct nulls (between 0 and π), while the beampattern with the conventional approach has at most $M_1 M_2 - 1$ distinct nulls (between 0 and π). The fact that the global beampattern, $\mathcal{B}_\theta(\mathbf{h})$, can be expressed as the product of two beamformer beampatterns is an interesting property that can be exploited in the design of very flexible global beamformers.

Given that the first microphone is the reference, we can define the input signal-to-noise ratio (SNR) with respect to this reference as

$$\text{iSNR} = \frac{\phi_X}{\phi_{V_1}}. \quad (24)$$

The output SNR is defined [from the variance of Z , see (19)] as with

$$\begin{aligned} \text{oSNR}(\mathbf{h}) &= \phi_X \frac{|\mathbf{h}^H \mathbf{d}_0|^2}{\mathbf{h}^H \Phi_{\mathbf{v}} \mathbf{h}} \\ &= \frac{\phi_X}{\phi_{V_1}} \times \frac{|\mathbf{h}^H \mathbf{d}_0|^2}{\mathbf{h}^H \Gamma_{\mathbf{v}} \mathbf{h}}. \end{aligned} \quad (25)$$

The definition of the gain in SNR is obtained from the previous definitions, i.e.,

$$\begin{aligned} \mathcal{G}(\mathbf{h}) &= \frac{\text{oSNR}(\mathbf{h})}{\text{iSNR}} \\ &= \frac{|\mathbf{h}^H \mathbf{d}_0|^2}{\mathbf{h}^H \Gamma_{\mathbf{v}} \mathbf{h}}. \end{aligned} \quad (26)$$

One convenient way to evaluate the sensitivity of the global ULA to some of its imperfections (e.g., sensor noise, small deviations of the microphone characteristics and positions) is via the so-called white noise gain (WNG), which is defined by taking $\Gamma_{\mathbf{v}} = \mathbf{I}_M$ in (26), where \mathbf{I}_M is the $M \times M$ identity matrix, i.e.,

$$\begin{aligned} \mathcal{W}(\mathbf{h}) &= \frac{|\mathbf{h}^H \mathbf{d}_0|^2}{\mathbf{h}^H \mathbf{h}} \\ &= \frac{|\mathbf{h}_1^H \mathbf{d}_{1,0}|^2}{\mathbf{h}_1^H \mathbf{h}_1} \times \frac{|\mathbf{h}_2^H \mathbf{d}_{2,0}|^2}{\mathbf{h}_2^H \mathbf{h}_2} \\ &= \mathcal{W}_1(\mathbf{h}_1) \times \mathcal{W}_2(\mathbf{h}_2), \end{aligned} \quad (27)$$

where

$$\mathcal{W}_i(\mathbf{h}_i) = \frac{|\mathbf{h}_i^H \mathbf{d}_{i,0}|^2}{\mathbf{h}_i^H \mathbf{h}_i} \quad (28)$$

for $i = 1, 2$. Obviously, the WNG of the global ULA is simply the product of the WNGs of the first and second ULAs described in Section II. It is easy to check that

$$\mathcal{W}(\mathbf{h}) \leq M_1 M_2, \quad \forall \mathbf{h}. \quad (29)$$

Another important measure, which quantifies how the microphone array performs in the presence of reverberation (which can be assumed as diffuse noise) is the directivity factor (DF). Considering the spherically isotropic (diffuse) noise field, the DF is defined by taking $\Gamma_{\mathbf{v}} = \mathbf{\Gamma}$ in (26):

$$\mathcal{D}(\mathbf{h}) = \frac{|\mathbf{h}^H \mathbf{d}_0|^2}{\mathbf{h}^H \mathbf{\Gamma} \mathbf{h}}, \quad (30)$$

where $\mathbf{\Gamma}$ is defined in (12). It is clear that

$$\mathcal{D}(\mathbf{h}) \leq \mathbf{d}_0^H \mathbf{\Gamma}^{-1} \mathbf{d}_0, \quad \forall \mathbf{h}. \quad (31)$$

We observe that contrary to the beampattern and the WNG, the DF of the global ULA cannot be factorized as the product of the DFs of the two virtual ULAs, i.e.,

$$\mathcal{D}(\mathbf{h}) \neq \mathcal{D}_1(\mathbf{h}_1) \times \mathcal{D}_2(\mathbf{h}_2), \quad (32)$$

where

$$\mathcal{D}_i(\mathbf{h}_i) = \frac{|\mathbf{h}_i^H \mathbf{d}_{i,0}|^2}{\mathbf{h}_i^H \mathbf{\Gamma}_i \mathbf{h}_i}, \quad (33)$$

$$\mathbf{\Gamma}_i = \frac{1}{2} \int_0^\pi \mathbf{d}_{i,\theta} \mathbf{d}_{i,\theta}^H \sin \theta d\theta, \quad (34)$$

for $i = 1, 2$. The elements of the $M_i \times M_i$ matrix $\mathbf{\Gamma}_i(\omega)$ are given by

$$[\mathbf{\Gamma}_i(\omega)]_{mn} = \text{sinc}[(m-n)\varpi_i] \quad (35)$$

with $[\mathbf{\Gamma}_i(\omega)]_{mm} = 1$, $m = 1, 2, \dots, M_i$. In fact, one can verify that $\mathbf{\Gamma} \neq \mathbf{\Gamma}_1 \otimes \mathbf{\Gamma}_2$, that is why (32) is true in general.

One can check that

$$\mathbf{h}_1 \otimes \mathbf{h}_2 = (\mathbf{h}_1 \otimes \mathbf{I}_{M_2}) \mathbf{h}_2 \quad (36)$$

$$= (\mathbf{I}_{M_1} \otimes \mathbf{h}_2) \mathbf{h}_1, \quad (37)$$

where \mathbf{I}_{M_i} is the identity matrix of size $M_i \times M_i$ ($i = 1, 2$). Basically, the previous expressions, which separate \mathbf{h}_2 and \mathbf{h}_1 into matrix-vector products, are very helpful and convenient to use in the derivations of hypercardioid and supercardioid beamformers (see Sections V-C and V-D). When \mathbf{h}_2 is fixed, given, and satisfies the distortionless constraint, i.e., $\mathbf{h}_2^H \mathbf{d}_{2,0} = 1$; then, thanks to (37), we can write the DF as

$$\begin{aligned} \mathcal{D}(\mathbf{h}_1 | \mathbf{h}_2) &= \frac{|\mathcal{B}_{1,0}(\mathbf{h}_1)|^2}{\mathbf{h}_1^H \mathbf{\Gamma}_{\mathbf{h}_2} \mathbf{h}_1} \\ &= \frac{|\mathbf{h}_1^H \mathbf{d}_{1,0}|^2}{\mathbf{h}_1^H \mathbf{\Gamma}_{\mathbf{h}_2} \mathbf{h}_1}, \end{aligned} \quad (38)$$

where

$$\begin{aligned} \mathbf{\Gamma}_{\mathbf{h}_2} &= \frac{1}{2} \int_0^\pi \mathbf{d}_{1,\theta} \mathbf{d}_{1,\theta}^H |\mathcal{B}_{2,\theta}(\mathbf{h}_2)|^2 \sin \theta d\theta \\ &= (\mathbf{I}_{M_1} \otimes \mathbf{h}_2)^H \mathbf{\Gamma} (\mathbf{I}_{M_1} \otimes \mathbf{h}_2). \end{aligned} \quad (39)$$

In the same way, when \mathbf{h}_1 is fixed, given, and satisfies the distortionless constraint, i.e., $\mathbf{h}_1^H \mathbf{d}_{1,0} = 1$; then, thanks to (36), we can express the DF as

$$\begin{aligned} \mathcal{D}(\mathbf{h}_2 | \mathbf{h}_1) &= \frac{|\mathcal{B}_{2,0}(\mathbf{h}_2)|^2}{\mathbf{h}_2^H \mathbf{\Gamma}_{\mathbf{h}_1} \mathbf{h}_2} \\ &= \frac{|\mathbf{h}_2^H \mathbf{d}_{2,0}|^2}{\mathbf{h}_2^H \mathbf{\Gamma}_{\mathbf{h}_1} \mathbf{h}_2}, \end{aligned} \quad (40)$$

where

$$\begin{aligned} \mathbf{\Gamma}_{\mathbf{h}_1} &= \frac{1}{2} \int_0^\pi \mathbf{d}_{2,\theta} \mathbf{d}_{2,\theta}^H |\mathcal{B}_{1,\theta}(\mathbf{h}_1)|^2 \sin \theta d\theta \\ &= (\mathbf{h}_1 \otimes \mathbf{I}_{M_2})^H \mathbf{\Gamma} (\mathbf{h}_1 \otimes \mathbf{I}_{M_2}). \end{aligned} \quad (41)$$

Another measure of interest in this study is the front-to-back ratio (FBR), which is defined as the ratio of the power of the output of the array to signals propagating from the front-half plane to the output power for signals arriving from the rear-half plane [15]. This ratio, for the spherically isotropic (diffuse)

noise field, is mathematically defined as [15]

$$\begin{aligned}\mathcal{F}(\mathbf{h}) &= \frac{\int_0^{\pi/2} |\mathcal{B}_\theta(\mathbf{h})|^2 \sin \theta d\theta}{\int_{\pi/2}^\pi |\mathcal{B}_\theta(\mathbf{h})|^2 \sin \theta d\theta} \\ &= \frac{\int_0^{\pi/2} |\mathcal{B}_{1,\theta}(\mathbf{h}_1)|^2 |\mathcal{B}_{2,\theta}(\mathbf{h}_2)|^2 \sin \theta d\theta}{\int_{\pi/2}^\pi |\mathcal{B}_{1,\theta}(\mathbf{h}_1)|^2 |\mathcal{B}_{2,\theta}(\mathbf{h}_2)|^2 \sin \theta d\theta} \\ &= \frac{\mathbf{h}^H \mathbf{\Gamma}_f \mathbf{h}}{\mathbf{h}^H \mathbf{\Gamma}_b \mathbf{h}},\end{aligned}\quad (42)$$

where

$$\mathbf{\Gamma}_f = \int_0^{\pi/2} \mathbf{d}_\theta \mathbf{d}_\theta^H \sin \theta d\theta, \quad (43)$$

$$\mathbf{\Gamma}_b = \int_{\pi/2}^\pi \mathbf{d}_\theta \mathbf{d}_\theta^H \sin \theta d\theta. \quad (44)$$

It can be verified that the elements of the $M \times M$ matrices $\mathbf{\Gamma}_f(\omega)$ and $\mathbf{\Gamma}_b(\omega)$ are given, respectively, by

$$[\mathbf{\Gamma}_f(\omega)]_{mn} = \frac{e^{j(n-m)\varpi} - 1}{j(n-m)\varpi} \quad (45)$$

and

$$[\mathbf{\Gamma}_b(\omega)]_{mn} = \frac{1 - e^{-j(n-m)\varpi}}{j(n-m)\varpi}, \quad (46)$$

with $[\mathbf{\Gamma}_f(\omega)]_{mm} = [\mathbf{\Gamma}_b(\omega)]_{mm} = 1$, $m = 1, 2, \dots, M$. Same as the DF, the FBR of the global ULA is not equal to the product of the FBRs of the two virtual ULAs, i.e.,

$$\mathcal{F}(\mathbf{h}) \neq \mathcal{F}_1(\mathbf{h}_1) \times \mathcal{F}_2(\mathbf{h}_2), \quad (47)$$

where

$$\begin{aligned}\mathcal{F}_i(\mathbf{h}_i) &= \frac{\int_0^{\pi/2} |\mathcal{B}_{i,\theta}(\mathbf{h}_i)|^2 \sin \theta d\theta}{\int_{\pi/2}^\pi |\mathcal{B}_{i,\theta}(\mathbf{h}_i)|^2 \sin \theta d\theta} \\ &= \frac{\mathbf{h}_i^H \mathbf{\Gamma}_{f,i} \mathbf{h}_i}{\mathbf{h}_i^H \mathbf{\Gamma}_{b,i} \mathbf{h}_i},\end{aligned}\quad (48)$$

with

$$\mathbf{\Gamma}_{f,i} = \int_0^{\pi/2} \mathbf{d}_{i,\theta} \mathbf{d}_{i,\theta}^H \sin \theta d\theta, \quad (49)$$

$$\mathbf{\Gamma}_{b,i} = \int_{\pi/2}^\pi \mathbf{d}_{i,\theta} \mathbf{d}_{i,\theta}^H \sin \theta d\theta, \quad (50)$$

for $i = 1, 2$. The elements of the $M_i \times M_i$ matrices $\mathbf{\Gamma}_{f,i}(\omega)$ and $\mathbf{\Gamma}_{b,i}(\omega)$ are given by

$$[\mathbf{\Gamma}_{f,i}(\omega)]_{mn} = \frac{e^{j(n-m)\varpi_i} - 1}{j(n-m)\varpi_i}, \quad (51)$$

$$[\mathbf{\Gamma}_{b,i}(\omega)]_{mn} = \frac{1 - e^{-j(n-m)\varpi_i}}{j(n-m)\varpi_i}, \quad (52)$$

with $[\mathbf{\Gamma}_{f,i}(\omega)]_{mm} = [\mathbf{\Gamma}_{b,i}(\omega)]_{mm} = 1$, $m = 1, 2, \dots, M_i$.

When \mathbf{h}_2 is fixed and given, and thanks to (37), we can write the FBR as

$$\mathcal{F}(\mathbf{h}_1|\mathbf{h}_2) = \frac{\mathbf{h}_1^H \mathbf{\Gamma}_{f,\mathbf{h}_2} \mathbf{h}_1}{\mathbf{h}_1^H \mathbf{\Gamma}_{b,\mathbf{h}_2} \mathbf{h}_1}, \quad (53)$$

where

$$\mathbf{\Gamma}_{f,\mathbf{h}_2} = \int_0^{\pi/2} \mathbf{d}_{1,\theta} \mathbf{d}_{1,\theta}^H |\mathcal{B}_{2,\theta}(\mathbf{h}_2)|^2 \sin \theta d\theta \quad (54)$$

$$= (\mathbf{I}_{M_1} \otimes \mathbf{h}_2)^H \mathbf{\Gamma}_f (\mathbf{I}_{M_1} \otimes \mathbf{h}_2),$$

$$\begin{aligned}\mathbf{\Gamma}_{b,\mathbf{h}_2} &= \int_{\pi/2}^\pi \mathbf{d}_{1,\theta} \mathbf{d}_{1,\theta}^H |\mathcal{B}_{2,\theta}(\mathbf{h}_2)|^2 \sin \theta d\theta \\ &= (\mathbf{I}_{M_1} \otimes \mathbf{h}_2)^H \mathbf{\Gamma}_b (\mathbf{I}_{M_1} \otimes \mathbf{h}_2).\end{aligned}\quad (55)$$

In the same way, when \mathbf{h}_1 is fixed and given, and thanks to (36), we can write the FBR as

$$\mathcal{F}(\mathbf{h}_2|\mathbf{h}_1) = \frac{\mathbf{h}_2^H \mathbf{\Gamma}_{f,\mathbf{h}_1} \mathbf{h}_2}{\mathbf{h}_2^H \mathbf{\Gamma}_{b,\mathbf{h}_1} \mathbf{h}_2}, \quad (56)$$

where

$$\mathbf{\Gamma}_{f,\mathbf{h}_1} = \int_0^{\pi/2} \mathbf{d}_{2,\theta} \mathbf{d}_{2,\theta}^H |\mathcal{B}_{1,\theta}(\mathbf{h}_1)|^2 \sin \theta d\theta \quad (57)$$

$$= (\mathbf{h}_1 \otimes \mathbf{I}_{M_2})^H \mathbf{\Gamma}_f (\mathbf{h}_1 \otimes \mathbf{I}_{M_2}),$$

$$\begin{aligned}\mathbf{\Gamma}_{b,\mathbf{h}_1} &= \int_{\pi/2}^\pi \mathbf{d}_{2,\theta} \mathbf{d}_{2,\theta}^H |\mathcal{B}_{1,\theta}(\mathbf{h}_1)|^2 \sin \theta d\theta \\ &= (\mathbf{h}_1 \otimes \mathbf{I}_{M_2})^H \mathbf{\Gamma}_b (\mathbf{h}_1 \otimes \mathbf{I}_{M_2}).\end{aligned}\quad (58)$$

V. DIFFERENTIAL BEAMFORMERS

In this section, we derive some useful examples of differential KP beamformers. Of course, many more can be deduced depending on the applications at hand.

A. Cardioid

The $(M_2 - 1)$ th-order cardioid has a unique null of multiplicity $M_2 - 1$ in the direction π . Therefore, the i th derivative, with $i = 0, 1, \dots, M_2 - 2$, of the beampattern of \mathbf{h}_2 with respect to $\cos \theta$ is equal to 0 at $\cos \theta = -1$, i.e.,

$$\left. \frac{d^i \mathcal{B}_{2,\theta}(\mathbf{h}_2)}{d \cos^i \theta} \right|_{\cos \theta = -1} = \mathcal{B}_{2,\pi}^{[i]}(\mathbf{h}_2) = 0, \quad (59)$$

with

$$\mathcal{B}_{2,\pi}^{[0]}(\mathbf{h}_2) = \mathcal{B}_{2,\pi}(\mathbf{h}_2).$$

We easily find that

$$\mathcal{B}_{2,\pi}^{[i]}(\mathbf{h}_2) = (j\omega\delta/c)^i (\mathbf{\Sigma}^i \mathbf{d}_{2,\pi})^H \mathbf{h}_2, \quad (60)$$

where

$$\mathbf{\Sigma} = \text{diag}(0, 1, \dots, M_2 - 1) \quad (61)$$

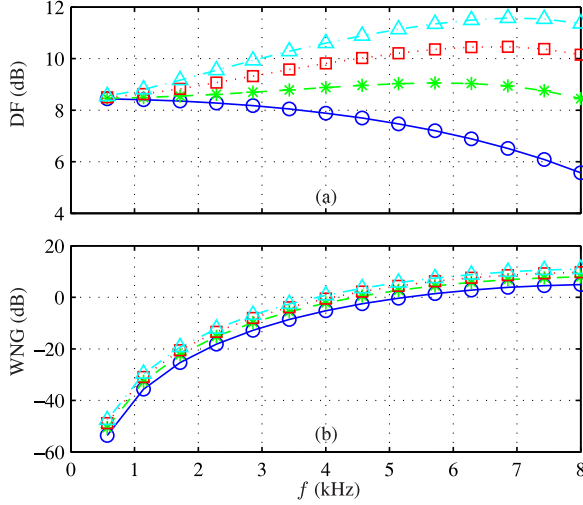


Fig. 2. Performances of the traditional third-order cardioid, $\mathbf{h}_{2,C}$, (solid line with circles) and the third-order KP cardioid, \mathbf{h}_C , as a function of frequency for $\delta = 1$ cm, $M_2 = 4$, and several values of M_1 : $M_1 = 2$ (dashed line with asterisks), $M_1 = 3$ (dotted line with squares), and $M_1 = 4$ (dash-dot line with triangles). (a) DF. (b) WNG.

is a diagonal matrix of size $M_2 \times M_2$. Combining the distortionless constraint, i.e.,

$$\mathcal{B}_{2,0}(\mathbf{h}_2) = \mathbf{d}_{2,0}^H \mathbf{h}_2 = 1, \quad (62)$$

with the $M_2 - 1$ equations from (59), we obtain a linear system of M_2 equations with M_2 unknowns:

$$\mathbf{D}_{2,\pi}^H \mathbf{h}_2 = \mathbf{i}, \quad (63)$$

where

$$\mathbf{D}_{2,\pi}^H = \begin{bmatrix} \mathbf{d}_{2,0}^H \\ (\Sigma^0 \mathbf{d}_{2,\pi})^H \\ (\Sigma^1 \mathbf{d}_{2,\pi})^H \\ \vdots \\ (\Sigma^{M_2-2} \mathbf{d}_{2,\pi})^H \end{bmatrix} \quad (64)$$

and \mathbf{i} is the first column of \mathbf{I}_{M_2} . Therefore, the cardioid of order $M_2 - 1$ at the second ULA is

$$\mathbf{h}_{2,C} = \mathbf{D}_{2,\pi}^{-H} \mathbf{i}. \quad (65)$$

For the first filter, we may take the DS beamformer, i.e.,

$$\mathbf{h}_{1,DS} = \frac{\mathbf{d}_{1,0}}{M_1}, \quad (66)$$

which maximizes the WNG. As a result, the $(M_2 - 1)$ th-order KP cardioid is

$$\mathbf{h}_C = \mathbf{h}_{1,DS} \otimes \mathbf{h}_{2,C}. \quad (67)$$

Figure 2 shows plots of the DFs and WNGs of the traditional third-order cardioid, $\mathbf{h}_{2,C}$, and the third-order KP cardioid, \mathbf{h}_C , as a function of frequency for $\delta = 1$ cm, $M_2 = 4$, and several values of M_1 . We observe that the DFs and WNGs of the KP cardioids are higher than those of the traditional cardioid. Furthermore, the DFs and WNGs of the KP cardioids increase as we increase the numbers of microphones in ULA 1.

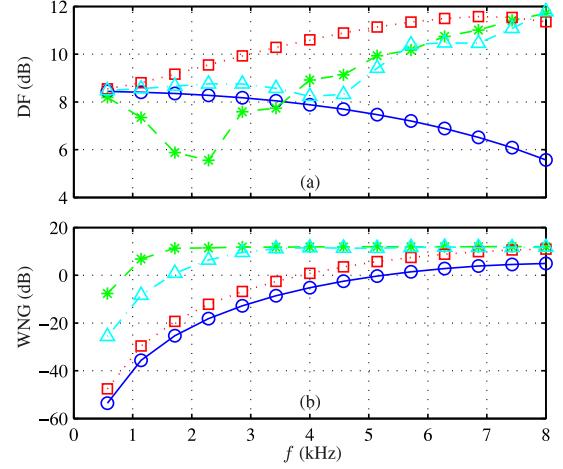


Fig. 3. Performances of different types of third-order cardioids as a function of frequency for $\delta = 1$ cm: traditional cardioid with $M = 4$ (solid line with circles), MN cardioid with $M = 16$ (dashed line with asterisks), KP cardioid with $M_1 = M_2 = 4$ (dotted line with squares), and KP cardioid with $M_1 = 2$ and $M_2 = 8$ (dash-dot line with triangles). (a) DF. (b) WNG.

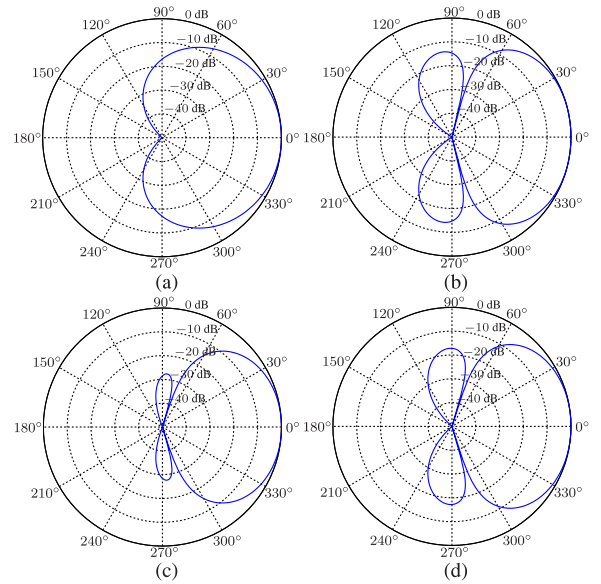


Fig. 4. Beampatterns of different types of third-order cardioids: (a) traditional cardioid with $M = 4$, (b) MN cardioid with $M = 16$, (c) KP cardioid with $M_1 = M_2 = 4$, and (d) KP cardioid with $M_1 = 2$ and $M_2 = 8$. Conditions: $\delta = 1$ cm and $f = 3$ kHz.

Clearly, the increase in both the DF and WNG is achieved at the expense of increasing M , the total number of microphones in the array. Therefore, we also compare the KP cardioids to the minimum-norm (MN) cardioid [8], [11], which employs M microphones ($M > M_2$) to design an $(M_2 - 1)$ th-order cardioid. Figure 3 shows plots of the DFs and WNGs of the third-order MN cardioid with $M = 16$, third-order KP cardioid with $M_1 = M_2 = 4$, and third-order KP cardioid with $M_1 = 2$ and $M_2 = 8$. Figure 4 displays the patterns of the corresponding third-order cardioids for $f = 3$ kHz. We observe that the MN cardioid achieves the maximum WNG, but for low frequencies its DF drops even below the traditional cardioid (which employs

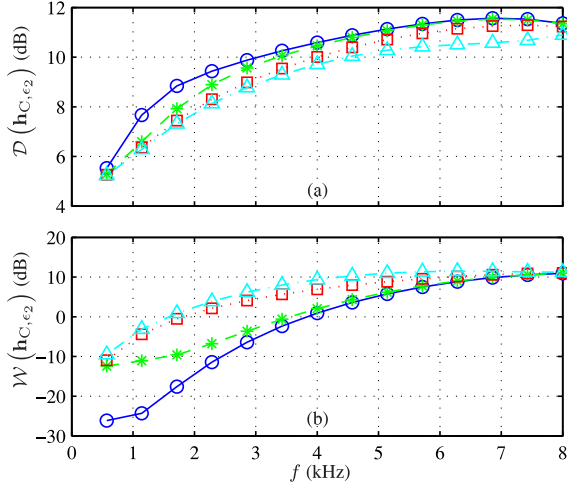


Fig. 5. Performance of the third-order robust KP cardioid, $\mathbf{h}_{C, \epsilon_2}$, as a function of frequency for $\delta = 1$ cm, $M_1 = 4$, $M_2 = 4$, and several values of ϵ_2 : $\epsilon_2 = 0.001$ (solid line with circles), $\epsilon_2 = 0.01$ (dashed line with asterisks), $\epsilon_2 = 0.1$ (dotted line with squares), and $\epsilon_2 = 1$ (dash-dot line with triangles). (a) DF. (b) WNG.

only $M = 4$ microphones). The KP cardioids, on the other hand, provide a more moderate increase in the WNG compared with the traditional cardioid, while also increasing the DF. Compared with the MN cardioid, the KP cardioids enable more flexibility in compromising the trade-off between WNG and DF.

To get a more robust beamformer, with higher WNG, we may optimize

$$\min_{\mathbf{h}_2} \mathbf{h}_2^H (\mathbf{D}'_{2,\pi} \mathbf{D}'_{2,\pi}{}^H + \epsilon_2 \mathbf{I}_{M_2}) \mathbf{h}_2 \quad \text{subject to} \quad \mathbf{C}_{2,\pi}^H \mathbf{h}_2 = \mathbf{i}_c, \quad (68)$$

where

$$\mathbf{D}'_{2,\pi} = [\boldsymbol{\Sigma}^1 \mathbf{d}_{2,\pi} \quad \boldsymbol{\Sigma}^2 \mathbf{d}_{2,\pi} \quad \dots \quad \boldsymbol{\Sigma}^{M_2-2} \mathbf{d}_{2,\pi}] \quad (69)$$

is a matrix of size $M_2 \times (M_2 - 2)$, $\epsilon_2 \geq 0$ is the regularization parameter,

$$\mathbf{C}_{2,\pi}^H = \begin{bmatrix} \mathbf{d}_{2,0}^H \\ \mathbf{d}_{2,\pi}^H \end{bmatrix} \quad (70)$$

is the constraint matrix of size $2 \times M_2$, and

$$\mathbf{i}_c = [1 \ 0]^T \quad (71)$$

is a vector of length 2. We see that with $\mathbf{C}_{2,\pi}$, the two main constraints are fulfilled, i.e., the distortionless one and a null in the direction π . We find that the optimal filter is

$$\begin{aligned} \mathbf{h}_{2,C,\epsilon_2} &= (\mathbf{D}'_{2,\pi} \mathbf{D}'_{2,\pi}{}^H + \epsilon_2 \mathbf{I}_{M_2})^{-1} \mathbf{C}_{2,\pi} \\ &\times \left[\mathbf{C}_{2,\pi}^H (\mathbf{D}'_{2,\pi} \mathbf{D}'_{2,\pi}{}^H + \epsilon_2 \mathbf{I}_{M_2})^{-1} \mathbf{C}_{2,\pi} \right]^{-1} \mathbf{i}_c. \end{aligned} \quad (72)$$

Therefore, the robust KP cardioid is

$$\mathbf{h}_{C,\epsilon_2} = \mathbf{h}_{1,DS} \otimes \mathbf{h}_{2,C,\epsilon_2}. \quad (73)$$

Figure 5 shows plots of the DFs and WNGs of the third-order robust KP cardioid, $\mathbf{h}_{C,\epsilon_2}$, as a function of frequency

for $\delta = 1$ cm, $M_1 = 4$, $M_2 = 4$, and several values of ϵ_2 . We observe that the WNG increases as we increase ϵ_2 , but the DF decreases.

B. Dipole

The design of the KP dipole is a bit different from the design of the KP cardioid as explained below.

The dipole of order $M_2 - 1$ has also a unique null of multiplicity $M_2 - 1$ but in the direction $\pi/2$. Since we have a null with maximum multiplicity, the i th ($i = 0, 1, \dots, M_2 - 2$) derivative of the beampattern of \mathbf{h}_2 with respect to $\cos \theta$ is equal to 0 at $\cos(\pi/2) = 0$, i.e.,

$$\left. \frac{d^i \mathcal{B}_{2,\theta}(\mathbf{h}_2)}{d \cos^i \theta} \right|_{\cos \theta = 0} = \mathcal{B}_{2,\pi/2}^{[i]}(\mathbf{h}_2) = 0, \quad (74)$$

with

$$\mathcal{B}_{2,\pi/2}^{[0]}(\mathbf{h}_2) = \mathcal{B}_{2,\pi/2}(\mathbf{h}_2).$$

We get

$$\mathcal{B}_{2,\pi/2}^{[i]}(\mathbf{h}_2) = (j\omega\delta/c)^i (\boldsymbol{\Sigma}^i \mathbf{d}_{2,\pi/2})^H \mathbf{h}_2, \quad (75)$$

where $\boldsymbol{\Sigma}$ is defined in (61). Combining the distortionless constraint with the $M_2 - 1$ constraints from (74), we have

$$\mathbf{D}_{2,\pi/2}^H \mathbf{h}_2 = \mathbf{i}, \quad (76)$$

where

$$\mathbf{D}_{2,\pi/2}^H = \begin{bmatrix} \mathbf{d}_{2,0}^H \\ (\boldsymbol{\Sigma}^0 \mathbf{d}_{2,\pi/2})^H \\ (\boldsymbol{\Sigma}^1 \mathbf{d}_{2,\pi/2})^H \\ \vdots \\ (\boldsymbol{\Sigma}^{M_2-2} \mathbf{d}_{2,\pi/2})^H \end{bmatrix}. \quad (77)$$

As a result, the dipole of order $M_2 - 1$ at the second ULA is

$$\mathbf{h}_{2,D} = \mathbf{D}_{2,\pi/2}^{-H} \mathbf{i}. \quad (78)$$

Another feature of the dipole is that it has a 1 in the direction π . To ensure that the global beampattern has also a 1 at π , we must add this constraint in the design of the first filter. We deduce that the constraint equation for \mathbf{h}_1 is

$$\mathbf{C}_{1,\pi}^H \mathbf{h}_1 = \begin{bmatrix} 1 \\ 1 \end{bmatrix}, \quad (79)$$

where

$$\mathbf{C}_{1,\pi}^H = \begin{bmatrix} \mathbf{d}_{1,0}^H \\ \mathbf{d}_{1,\pi}^H \end{bmatrix} \quad (80)$$

is the constraint matrix of size $2 \times M_1$. Since we want to maximize the WNG of \mathbf{h}_1 subject to (79), we find the MN beamformer:

$$\mathbf{h}_{1,MN} = \mathbf{C}_{1,\pi} (\mathbf{C}_{1,\pi}^H \mathbf{C}_{1,\pi})^{-1} \begin{bmatrix} 1 \\ 1 \end{bmatrix}. \quad (81)$$

Now, that the two filters are derived, we deduce that the robust $(M_2 - 1)$ th-order KP dipole is

$$\mathbf{h}_D = \mathbf{h}_{1,MN} \otimes \mathbf{h}_{2,D}. \quad (82)$$

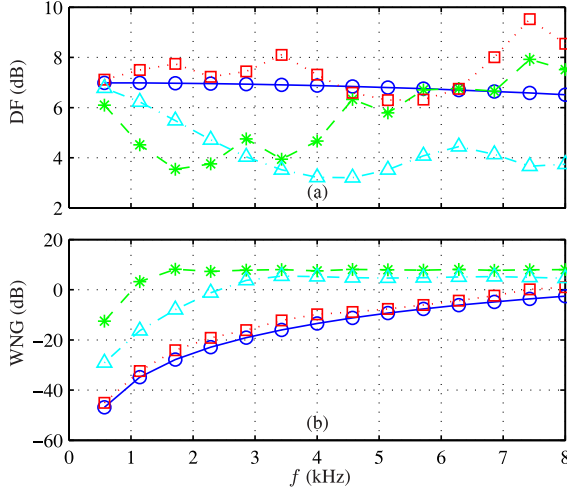


Fig. 6. Performances of different types of robust second-order dipoles as a function of frequency for $\delta = 1$ cm: traditional dipole, $\mathbf{h}_{2,D,\epsilon_2}$, with $M = 3$ (solid line with circles), MN dipole with $M = 12$ (dashed line with asterisks), KP dipole, $\mathbf{h}_{D,\epsilon_2}$, with $M_1 = 4$ and $M_2 = 3$ (dotted line with squares), and KP dipole with $M_1 = 2$ and $M_2 = 6$ (dash-dot line with triangles). (a) DF. (b) WNG.

As we did for the cardioid, we can derive a robust KP dipole:

$$\mathbf{h}_{D,\epsilon_2} = \mathbf{h}_{1,MN} \otimes \mathbf{h}_{2,D,\epsilon_2}, \quad (83)$$

where

$$\begin{aligned} \mathbf{h}_{2,D,\epsilon_2} &= \left(\mathbf{D}'_{2,\pi/2} \mathbf{D}'_{2,\pi/2}{}^H + \epsilon_2 \mathbf{I}_{M_2} \right)^{-1} \mathbf{C}_{2,\pi/2} \\ &\times \left[\mathbf{C}_{2,\pi/2}{}^H \left(\mathbf{D}'_{2,\pi/2} \mathbf{D}'_{2,\pi/2}{}^H + \epsilon_2 \mathbf{I}_{M_2} \right)^{-1} \mathbf{C}_{2,\pi/2} \right]^{-1} \mathbf{i}_c, \end{aligned} \quad (84)$$

with

$$\mathbf{D}'_{2,\pi/2} = \left[\Sigma^1 \mathbf{d}_{2,\pi/2} \quad \Sigma^2 \mathbf{d}_{2,\pi/2} \quad \cdots \quad \Sigma^{M_2-2} \mathbf{d}_{2,\pi/2} \right] \quad (85)$$

and

$$\mathbf{C}_{2,\pi/2}{}^H = \begin{bmatrix} \mathbf{d}_{2,0}{}^H \\ \mathbf{d}_{2,\pi/2}{}^H \end{bmatrix}. \quad (86)$$

Figure 6 shows plots of the DFs and WNGs of different types of robust second-order dipoles as a function of frequency for $\delta = 1$ cm and $\epsilon_2 = 10^{-8}$, including the traditional dipole, $\mathbf{h}_{2,D,\epsilon_2}$, with $M = 3$, MN dipole with $M = 12$ [8], [11], KP dipole, $\mathbf{h}_{D,\epsilon_2}$, with $M_1 = 4$ and $M_2 = 3$, and KP dipole with $M_1 = 2$ and $M_2 = 6$. Figure 7 displays the patterns of the corresponding robust second-order dipoles for $f = 3$ kHz. We observe that the MN dipole achieves the maximum WNG, but its DF for low frequencies is the worst. Compared with the traditional dipole, the KP dipoles provide a more moderate increase in the WNG than the MN dipole, and different variations of the DFs as a function of frequency, which may be useful in some applications.

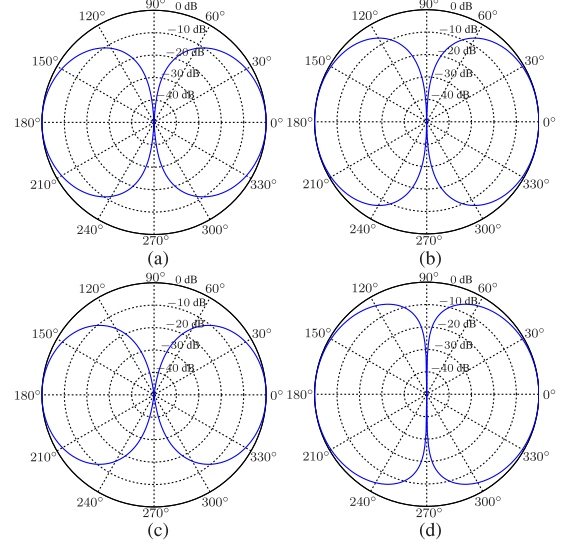


Fig. 7. Beampatterns of different types of robust second-order dipoles: (a) traditional dipole with $M = 3$, (b) MN dipole with $M = 12$, (c) KP dipole with $M_1 = 4$ and $M_2 = 3$, and (d) KP dipole with $M_1 = 2$ and $M_2 = 6$. Conditions: $\delta = 1$ cm and $f = 3$ kHz.

C. Hypercardioid

The hypercardioid is usually obtained by maximizing $\mathcal{D}(\mathbf{h})$ in (30). But this DF cannot be maximized directly and an iterative algorithm is needed.

We start by taking the hypercardioid of order $M_2 - 1$ at the second ULA, i.e.,

$$\mathbf{h}_2^{(0)} = \frac{\Gamma_2^{-1} \mathbf{d}_{2,0}}{\mathbf{d}_{2,0}{}^H \Gamma_2^{-1} \mathbf{d}_{2,0}}. \quad (87)$$

Substituting $\mathbf{h}_2^{(0)}$ into (39), we get

$$\Gamma_{\mathbf{h}_2^{(0)}} = \left(\mathbf{I}_{M_1} \otimes \mathbf{h}_2^{(0)} \right)^H \Gamma \left(\mathbf{I}_{M_1} \otimes \mathbf{h}_2^{(0)} \right). \quad (88)$$

Now, substituting this expression into the DF in (38), we obtain at iteration 1:

$$\mathcal{D}(\mathbf{h}_1^{(1)} | \mathbf{h}_2^{(0)}) = \frac{\left| \left(\mathbf{h}_1^{(1)} \right)^H \mathbf{d}_{1,0} \right|^2}{\left(\mathbf{h}_1^{(1)} \right)^H \Gamma_{\mathbf{h}_2^{(0)}} \mathbf{h}_1^{(1)}}. \quad (89)$$

The maximization of $\mathcal{D}(\mathbf{h}_1^{(1)} | \mathbf{h}_2^{(0)})$ with respect to $\mathbf{h}_1^{(1)}$ gives

$$\mathbf{h}_1^{(1)} = \frac{\Gamma_{\mathbf{h}_2^{(0)}}^{-1} \mathbf{d}_{1,0}}{\mathbf{d}_{1,0}{}^H \Gamma_{\mathbf{h}_2^{(0)}}^{-1} \mathbf{d}_{1,0}}. \quad (90)$$

Using $\mathbf{h}_1^{(1)}$ in (41), we get

$$\Gamma_{\mathbf{h}_1^{(1)}} = \left(\mathbf{h}_1^{(1)} \otimes \mathbf{I}_{M_2} \right)^H \Gamma \left(\mathbf{h}_1^{(1)} \otimes \mathbf{I}_{M_2} \right). \quad (91)$$

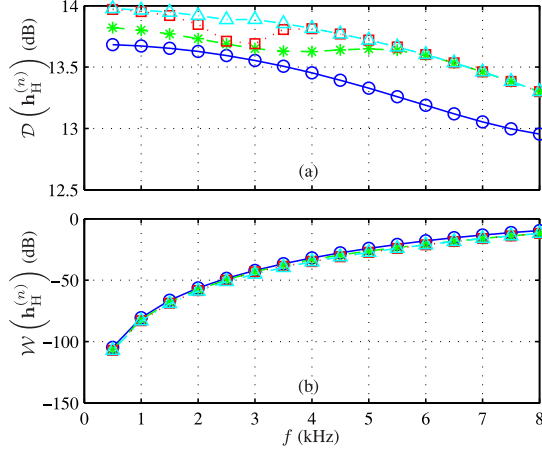


Fig. 8. Performance of the KP hypercardioid, $\mathbf{h}_H^{(n)}$, as a function of frequency for $M_1 = M_2 = 3$, $\delta = 5$ mm, and several values of n : $n = 1$ (solid line with circles), $n = 2$ (dashed line with asterisks), $n = 3$ (dotted line with squares), and $n = 10$ (dash-dot line with triangles). (a) DF. (b) WNG.

As a result, the DF in (40) is

$$\mathcal{D}(\mathbf{h}_2^{(1)}|\mathbf{h}_1^{(1)}) = \frac{\left| \left(\mathbf{h}_2^{(1)} \right)^H \mathbf{d}_{2,0} \right|^2}{\left(\mathbf{h}_2^{(1)} \right)^H \mathbf{\Gamma}_{\mathbf{h}_1^{(1)}} \mathbf{h}_2^{(1)}}, \quad (92)$$

whose maximization with respect to $\mathbf{h}_2^{(1)}$ gives

$$\mathbf{h}_2^{(1)} = \frac{\mathbf{\Gamma}_{\mathbf{h}_1^{(1)}}^{-1} \mathbf{d}_{2,0}}{\mathbf{d}_{2,0}^H \mathbf{\Gamma}_{\mathbf{h}_1^{(1)}}^{-1} \mathbf{d}_{2,0}}. \quad (93)$$

Continuing the iterations up to the iteration n , we easily get for the first filter:

$$\mathbf{h}_1^{(n)} = \frac{\mathbf{\Gamma}_{\mathbf{h}_2^{(n-1)}}^{-1} \mathbf{d}_{1,0}}{\mathbf{d}_{1,0}^H \mathbf{\Gamma}_{\mathbf{h}_2^{(n-1)}}^{-1} \mathbf{d}_{1,0}}, \quad (94)$$

with

$$\mathbf{\Gamma}_{\mathbf{h}_2^{(n-1)}} = \left(\mathbf{I}_{M_1} \otimes \mathbf{h}_2^{(n-1)} \right)^H \mathbf{\Gamma} \left(\mathbf{I}_{M_1} \otimes \mathbf{h}_2^{(n-1)} \right), \quad (95)$$

and for the second filter:

$$\mathbf{h}_2^{(n)} = \frac{\mathbf{\Gamma}_{\mathbf{h}_1^{(n)}}^{-1} \mathbf{d}_{2,0}}{\mathbf{d}_{2,0}^H \mathbf{\Gamma}_{\mathbf{h}_1^{(n)}}^{-1} \mathbf{d}_{2,0}}, \quad (96)$$

with

$$\mathbf{\Gamma}_{\mathbf{h}_1^{(n)}} = \left(\mathbf{h}_1^{(n)} \otimes \mathbf{I}_{M_2} \right)^H \mathbf{\Gamma} \left(\mathbf{h}_1^{(n)} \otimes \mathbf{I}_{M_2} \right). \quad (97)$$

Finally, we deduce that the KP hypercardioid is at iteration n :

$$\mathbf{h}_H^{(n)} = \mathbf{h}_1^{(n)} \otimes \mathbf{h}_2^{(n)}. \quad (98)$$

Figure 8 shows plots of the DFs and WNGs of the KP hypercardioid, $\mathbf{h}_H^{(n)}$, as a function of frequency for $M_1 = M_2 = 3$, $\delta = 5$ mm, and several values of n . We observe that the DF of the KP hypercardioid increases at each iteration, and roughly

converges after five iterations, while the WNG decreases at each iteration.

D. Supercardioid

The supercardioid is obtained by maximizing the FBR. To fully maximize the FBR in (42), we need to derive an iterative algorithm.

At iteration 0, we may take the supercardioid of order $M_2 - 1$ at the second ULA, i.e.,

$$\mathbf{h}_2^{(0)} = \frac{\mathbf{t}_2}{\mathbf{d}_{2,0}^H \mathbf{t}_2}, \quad (99)$$

where \mathbf{t}_2 is the eigenvector corresponding to the maximum eigenvalue of the matrix $\mathbf{\Gamma}_{\mathbf{b}_2}^{-1} \mathbf{\Gamma}_{\mathbf{f},2}$. Substituting $\mathbf{h}_2^{(0)}$ into (54) and (55), we get

$$\mathbf{\Gamma}_{\mathbf{f},\mathbf{h}_2^{(0)}} = \left(\mathbf{I}_{M_1} \otimes \mathbf{h}_2^{(0)} \right)^H \mathbf{\Gamma}_f \left(\mathbf{I}_{M_1} \otimes \mathbf{h}_2^{(0)} \right), \quad (100)$$

$$\mathbf{\Gamma}_{\mathbf{b},\mathbf{h}_2^{(0)}} = \left(\mathbf{I}_{M_1} \otimes \mathbf{h}_2^{(0)} \right)^H \mathbf{\Gamma}_b \left(\mathbf{I}_{M_1} \otimes \mathbf{h}_2^{(0)} \right). \quad (101)$$

Now, plugging these expressions into the FBR in (53), we obtain at iteration 1:

$$\mathcal{F}(\mathbf{h}_1^{(1)}|\mathbf{h}_2^{(0)}) = \frac{\left(\mathbf{h}_1^{(1)} \right)^H \mathbf{\Gamma}_{\mathbf{f},\mathbf{h}_2^{(0)}} \mathbf{h}_1^{(1)}}{\left(\mathbf{h}_1^{(1)} \right)^H \mathbf{\Gamma}_{\mathbf{b},\mathbf{h}_2^{(0)}} \mathbf{h}_1^{(1)}}. \quad (102)$$

The maximization of $\mathcal{F}(\mathbf{h}_1^{(1)}|\mathbf{h}_2^{(0)})$ with respect of $\mathbf{h}_1^{(1)}$ leads to

$$\mathbf{h}_1^{(1)} = \frac{\mathbf{t}_1^{(0)}}{\mathbf{d}_{1,0}^H \mathbf{t}_1^{(0)}}, \quad (103)$$

where $\mathbf{t}_1^{(0)}$ is the eigenvector corresponding to the maximum eigenvalue of the matrix $\mathbf{\Gamma}_{\mathbf{b},\mathbf{h}_2^{(0)}}^{-1} \mathbf{\Gamma}_{\mathbf{f},\mathbf{h}_2^{(0)}}$. Using $\mathbf{h}_1^{(1)}$ in (57) and (58), we get

$$\mathbf{\Gamma}_{\mathbf{f},\mathbf{h}_1^{(1)}} = \left(\mathbf{h}_1^{(1)} \otimes \mathbf{I}_{M_2} \right)^H \mathbf{\Gamma}_f \left(\mathbf{h}_1^{(1)} \otimes \mathbf{I}_{M_2} \right), \quad (104)$$

$$\mathbf{\Gamma}_{\mathbf{b},\mathbf{h}_1^{(1)}} = \left(\mathbf{h}_1^{(1)} \otimes \mathbf{I}_{M_2} \right)^H \mathbf{\Gamma}_b \left(\mathbf{h}_1^{(1)} \otimes \mathbf{I}_{M_2} \right). \quad (105)$$

As a result, the FBR in (56) is

$$\mathcal{F}(\mathbf{h}_2^{(1)}|\mathbf{h}_1^{(1)}) = \frac{\left(\mathbf{h}_2^{(1)} \right)^H \mathbf{\Gamma}_{\mathbf{f},\mathbf{h}_1^{(1)}} \mathbf{h}_2^{(1)}}{\left(\mathbf{h}_2^{(1)} \right)^H \mathbf{\Gamma}_{\mathbf{b},\mathbf{h}_1^{(1)}} \mathbf{h}_2^{(1)}}, \quad (106)$$

whose maximization with respect to $\mathbf{h}_2^{(1)}$ gives

$$\mathbf{h}_2^{(1)} = \frac{\mathbf{t}_2^{(1)}}{\mathbf{d}_{2,0}^H \mathbf{t}_2^{(1)}}, \quad (107)$$

where $\mathbf{t}_2^{(1)}$ is the eigenvector corresponding to the maximum eigenvalue of the matrix $\mathbf{\Gamma}_{\mathbf{b},\mathbf{h}_1^{(1)}}^{-1} \mathbf{\Gamma}_{\mathbf{f},\mathbf{h}_1^{(1)}}$.

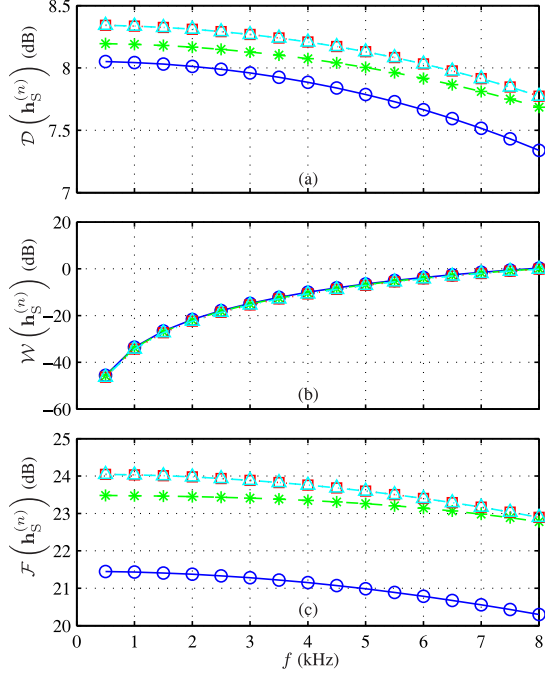


Fig. 9. Performance of the KP supercardioid, $\mathbf{h}_S^{(n)}$, as a function of frequency for $M_1 = M_2 = 2$, $\delta = 5$ mm, and several values of n : $n = 1$ (solid line with circles), $n = 2$ (dashed line with asterisks), $n = 3$ (dotted line with squares), and $n = 10$ (dash-dot line with triangles). (a) DF. (b) WNG. (c) FBR.

Continuing to iterate up to iteration n , we easily get for the first filter:

$$\mathbf{h}_1^{(n)} = \frac{\mathbf{t}_1^{(n-1)}}{\mathbf{d}_{1,0}^H \mathbf{t}_1^{(n-1)}}, \quad (108)$$

where $\mathbf{t}_1^{(n-1)}$ is the eigenvector corresponding to the maximum eigenvalue of the matrix $\Gamma_{\mathbf{b}, \mathbf{h}_2}^{-1(n-1)} \Gamma_{\mathbf{f}, \mathbf{h}_2}^{(n-1)}$, with

$$\Gamma_{\mathbf{f}, \mathbf{h}_2}^{(n-1)} = \left(\mathbf{I}_{M_1} \otimes \mathbf{h}_2^{(n-1)} \right)^H \Gamma_{\mathbf{f}} \left(\mathbf{I}_{M_1} \otimes \mathbf{h}_2^{(n-1)} \right), \quad (109)$$

$$\Gamma_{\mathbf{b}, \mathbf{h}_2}^{(n-1)} = \left(\mathbf{I}_{M_1} \otimes \mathbf{h}_2^{(n-1)} \right)^H \Gamma_{\mathbf{b}} \left(\mathbf{I}_{M_1} \otimes \mathbf{h}_2^{(n-1)} \right), \quad (110)$$

and for the second filter:

$$\mathbf{h}_2^{(n)} = \frac{\mathbf{t}_2^{(n)}}{\mathbf{d}_{2,0}^H \mathbf{t}_2^{(n)}}, \quad (111)$$

where $\mathbf{t}_2^{(n)}$ is the eigenvector corresponding to the maximum eigenvalue of the matrix $\Gamma_{\mathbf{b}, \mathbf{h}_1}^{-1(n)} \Gamma_{\mathbf{f}, \mathbf{h}_1}^{(n)}$, with

$$\Gamma_{\mathbf{f}, \mathbf{h}_1}^{(n)} = \left(\mathbf{h}_1^{(n)} \otimes \mathbf{I}_{M_2} \right)^H \Gamma_{\mathbf{f}} \left(\mathbf{h}_1^{(n)} \otimes \mathbf{I}_{M_2} \right), \quad (112)$$

$$\Gamma_{\mathbf{b}, \mathbf{h}_1}^{(n)} = \left(\mathbf{h}_1^{(n)} \otimes \mathbf{I}_{M_2} \right)^H \Gamma_{\mathbf{b}} \left(\mathbf{h}_1^{(n)} \otimes \mathbf{I}_{M_2} \right). \quad (113)$$

Finally, we deduce that the KP supercardioid is at iteration n :

$$\mathbf{h}_S^{(n)} = \mathbf{h}_1^{(n)} \otimes \mathbf{h}_2^{(n)}. \quad (114)$$

Figure 9 shows plots of the DFs, WNGs, and FBRs of the KP supercardioid, $\mathbf{h}_S^{(n)}$, as a function of frequency for $M_1 = M_2 =$

2 , $\delta = 5$ mm, and several values of n . We observe that the FBR of the KP supercardioid increases at each iteration, and roughly converges after three iterations, while the DF also increases at each iteration and the WNG remains almost the same.

VI. CONCLUSION

We have introduced differential Kronecker product beamforming based on Kronecker product decompositions of a physical array into two virtual arrays. We defined performance measures by using Kronecker product filters, and showed how to derive some useful examples of differential beamformers, namely the cardioid, dipole, hypercardioid, and supercardioid, using the Kronecker product formulation. We showed that the beampattern and the WNG of the global array can be expressed as the product of the counterparts of the two virtual arrays; but the DF and FBR cannot be factorized into a similar form and as a result these two measures cannot be maximized directly. Accordingly, we developed iterative algorithms for their maximization. The proposed approach enables much more flexibility in the design of differential beamformers, compared to the well-known and studied conventional approach. Furthermore, the proposed approach can be extended to other array structures and other beamformers, depending on the application at hand.

ACKNOWLEDGMENT

The authors would like to thank the associate editor and the anonymous reviewers for their constructive comments and useful suggestions.

REFERENCES

- [1] F. P. Ribeiro and V. H. Nascimento, "Fast transforms for acoustic imaging—Part I: Theory," *IEEE Trans. Image Process.*, vol. 20, no. 8, pp. 2229–2240, Aug. 2011.
- [2] V. H. Nascimento, M. C. Silva, and B. S. Masiero, "Acoustic image estimation using fast transforms," in *Proc. IEEE Sensor Array Multichannel Signal Process.*, Rio de Janeiro, Brazil, Jul. 2016, pp. 1–5.
- [3] L. N. Ribeiro, A. L. F. de Almeida, and J. C. M. Mota, "Identification of separable systems using trilinear filtering," in *Proc. IEEE 6th Int. Workshop Comput. Adv. Multi-Sensor Adapt. Process.*, Cancun, Mexico, Dec. 2015, pp. 189–192.
- [4] C. Paleologu, J. Benesty, and S. Ciochină, "Linear system identification based on a Kronecker product decomposition," *IEEE/ACM Trans. Audio, Speech, Lang. Process.*, vol. 26, no. 10, pp. 1793–1808, Oct. 2018.
- [5] Y. I. Abramovich, G. J. Frazer, and B. A. Johnson, "Iterative adaptive Kronecker MIMO radar beamformer: Description and convergence analysis," *IEEE Trans. Signal Process.*, vol. 58, no. 7, pp. 33 681–3691, Jul. 2010.
- [6] L. N. Ribeiro, A. L. F. de Almeida, and J. C. M. Mota, "Tensor beamforming for multilinear translation invariant arrays," in *Proc. IEEE Int. Conf. Acoust., Speech Signal Process.*, Shanghai, China, Mar. 2016, pp. 2966–2970.
- [7] G. W. Elko, "Superdirectional microphone arrays," in *Acoustic Signal Processing for Telecommunication*, S. L. Gay and J. Benesty, Eds. Boston, MA, USA: Kluwer, 2000, pp. 181–237, ch. 10.
- [8] J. Benesty and J. Chen, *Study and Design of Differential Microphone Arrays*. Berlin, Germany: Springer-Verlag, 2012.
- [9] J. Benesty, J. Chen, and I. Cohen, *Design of Circular Differential Microphone Arrays*. Switzerland: Springer-Verlag, 2015.
- [10] B. Masiero and V. H. Nascimento, "Revisiting the Kronecker array transform," *IEEE Signal Process. Lett.*, vol. 24, no. 5, pp. 525–529, May 2017.
- [11] J. Benesty, I. Cohen, and J. Chen, *Fundamentals of Signal Enhancement and Array Signal Processing*. Singapore: Wiley–IEEE Press, 2018.
- [12] D. H. Johnson and D. E. Dudgeon, *Array Signal Processing: Concepts and Techniques* (Signal Processing Series). Englewood Cliffs, NJ, USA: Prentice-Hall, 1993.

- [13] G. W. Elko and J. Meyer, "Microphone arrays," in *Springer Handbook of Speech Processing*, J. Benesty, M. M. Sondhi, and Y. Huang, Eds. Berlin, Germany: Springer-Verlag, 2008, pp. 1021–1041, ch. 50.
- [14] J. Benesty, J. Chen, and Y. Huang, *Microphone Array Signal Processing*. Berlin, Germany: Springer-Verlag, 2008.
- [15] R. N. Marshall and W. R. Harry, "A new microphone providing uniform directivity over an extended frequency range," *J. Acoust. Soc. Amer.*, vol. 12, pp. 481–497, 1941.



Israel Cohen (M'01–SM'03–F'15) received the B.Sc. (*summa cum laude*), M.Sc., and Ph.D. degrees in electrical engineering from the Technion–Israel Institute of Technology, Haifa, Israel, in 1990, 1993, and 1998, respectively.

He is currently a Professor in electrical engineering at the Technion–Israel Institute of Technology. He is also a Visiting Professor at Northwestern Polytechnical University, Xi'an, China. From 1990 to 1998, he was a Research Scientist with RAFAEL Research Laboratories, Haifa, Israel Ministry of Defense. From

1998 to 2001, he was a Postdoctoral Research Associate with the Computer Science Department, Yale University, New Haven, CT, USA. In 2001, he joined the Electrical Engineering Department, Technion. He is a co-editor of the Multichannel Speech Processing Section of the *Springer Handbook of Speech Processing* (Springer, 2008), and the coauthor of *Fundamentals of Signal Enhancement and Array Signal Processing* (Wiley-IEEE Press, 2018). His research interests are array processing, statistical signal processing, analysis and modeling of acoustic signals, speech enhancement, noise estimation, microphone arrays, source localization, blind source separation, system identification, and adaptive filtering.

Dr. Cohen is an Associate Member of the IEEE Audio and Acoustic Signal Processing Technical Committee and the Distinguished Lecturer of the IEEE Signal Processing Society. He was an Associate Editor for the IEEE TRANSACTIONS ON AUDIO, SPEECH, AND LANGUAGE PROCESSING and IEEE SIGNAL PROCESSING LETTERS and a Member of the IEEE Audio and Acoustic Signal Processing Technical Committee and the IEEE Speech and Language Processing Technical Committee. He was the recipient of the Norman Seiden Prize for Academic Excellence (2017), the SPS Signal Processing Letters Best Paper Award (2014), the Alexander Goldberg Prize for Excellence in Research (2010), and the Muriel and David Jacknow Award for Excellence in Teaching (2009).



Jacob Benesty received the Master degree in microwaves from Pierre & Marie Curie University, Paris, France, in 1987, and the Ph.D. degree in control and signal processing from Orsay University, Orsay, France, in April 1991. During the Ph.D. (from November 1989 to April 1991), he worked on adaptive filters and fast algorithms at the Centre National d'Etudes des Telecommunications, Paris, France. From January 1994 to July 1995, he worked at Telecom Paris University on multichannel adaptive filters and acoustic echo cancellation. From October 1995 to

May 2003, he was first a Consultant and then a Member of the Technical Staff at Bell Laboratories, Murray Hill, NJ, USA. In May 2003, he joined the University of Quebec, INRS-EMT, in Montreal, Quebec, Canada, as a Professor. He is also a Visiting Professor at the Technion, Haifa, Israel, an Adjunct Professor at Aalborg University, Denmark, and a Guest Professor at Northwestern Polytechnical University, Xi'an, China. He is the inventor of many important technologies. In particular, he was the lead researcher at Bell Labs who conceived and designed the world-first real-time hands-free full-duplex stereophonic teleconferencing system. Also, he conceived and designed the world-first PC-based multi-party hands-free full-duplex stereo conferencing system over IP networks. He is the editor of the book series Springer Topics in Signal Processing. He has co-authored and co-edited/co-authored numerous books in the area of acoustic signal processing. His research interests are in signal processing, acoustic signal processing, and multimedia communications.

Dr. Benesty was the General Chair and Technical Chair for many international conferences and a member of several IEEE technical committees. Four of his journal papers were awarded by the IEEE Signal processing Society and in 2010 he was the recipient of the Gheorghe Cartianu Award from the Romanian Academy.



Jingdong Chen (M'99–SM'09) received the Ph.D. degree in pattern recognition and intelligence control from the Chinese Academy of Sciences, Beijing, China, in 1998.

From 1998 to 1999, he was with ATR Interpreting Telecommunications Research Laboratories, Kyoto, Japan, where he conducted research on speech synthesis, speech analysis, as well as objective measurements for evaluating speech synthesis. He then joined the Griffith University, Brisbane, QLD, Australia, where he engaged in research on robust speech recognition and signal processing. From 2000 to 2001, he worked at ATR Spoken Language Translation Research Laboratories on robust speech recognition and speech enhancement. From 2001 to 2009, he was a Member of Technical Staff at Bell Laboratories, Murray Hill, NJ, USA, working on acoustic signal processing for telecommunications. He subsequently joined WeVoice, Inc., in New Jersey, serving as the Chief Scientist. He is currently a Professor at the Northwestern Polytechnical University, Xi'an, China. His research interests include acoustic signal processing, adaptive signal processing, speech enhancement, adaptive noise/echo control, microphone array signal processing, signal separation, and speech communication.

Dr. Chen was an Associate Editor for the IEEE TRANSACTIONS ON AUDIO, SPEECH, AND LANGUAGE PROCESSING from 2008 to 2014 and as a Technical Committee (TC) member of the IEEE Signal Processing Society (SPS) TC on Audio and Electroacoustics from 2007 to 2009. He is currently a Member of the IEEE SPS TC on Audio and Acoustic Signal Processing, and a member of the editorial advisory board of the *Open Signal Processing Journal*. He was the General Co-Chair of ACM WUWNET 2018 and IWAENC 2016, the Technical Program Chair of IEEE TENCON 2013, the Technical Program Co-Chair of IEEE WASPAA 2009, IEEE ChinaSIP 2014, IEEE ICSPCC 2014, and IEEE ICSPCC 2015, and helped in organizing many other conferences. He co-authored 12 monograph books including *Fundamentals of Signal Enhancement and Array Signal Processing* (Wiley, 2017), *Design of Circular Differential Microphone Arrays* (Springer, 2015), *Study and Design of Differential Microphone Arrays* (Springer, 2013), *Noise Reduction in Speech Processing* (Springer, 2009), *Microphone Array Signal Processing* (Springer, 2008), and *Acoustic MIMO Signal Processing* (Springer, 2006). He was the recipient of the 2008 Best Paper Award from the IEEE Signal Processing Society (with Benesty, Huang, and Doclo), the Best Paper Award from the IEEE Workshop on Applications of Signal Processing to Audio and Acoustics in 2011 (with Benesty), the Bell Labs Role Model Teamwork Award twice, respectively, in 2009 and 2007, the NASA Tech Brief Award twice, respectively, in 2010 and 2009, and the Young Author Best Paper Award at the 5th National Conference on Man-Machine Speech Communications in 1998. He is the co-author of a paper for which C. Pan received the IEEE R10 (Asia-Pacific Region) Distinguished Student Paper Award (First Prize) in 2016. He was also the recipient of the Japan Trust International Research Grant from the Japan Key Technology Center in 1998 and the "Distinguished Young Scientists Fund" from the National Natural Science Foundation of China in 2014.